Check for updates

ADVANCED MATERIALS
www.advmat.de

Highly Transparent and Self-Healable Solar Thermal Anti-/Deicing Surfaces: When Ultrathin MXene Multilayers Marry a Solid Slippery Self-Cleaning Coating

Wenwen Niu, George Y. Chen, Haolan Xu, Xiaokong Liu, and Junqi Sun*

Solar anti-/deicing can solve icing problems by converting sunlight into heat. One of the biggest problems, which has long been plaguing the design of solar anti-/deicing surfaces, is that photothermal materials are always lightproof and appear black, because of the mutual exclusiveness between generating heat and retaining transparency. Herein, a highly transparent and scalable solar anti-/deicing surface is reported, which enables the coated glass to exhibit high transparency (>77% transmittance at 550 nm) and meanwhile causes a >30 °C surface temperature increase relative to the ambient environment under 1.0 sun illumination. Such a transparent anti-/deicing surface can be fabricated onto a large class of substrates (e.g., glass, ceramics, metals, plastics), by applying a solid omniphobic slippery coating onto layer-by-layer-assembled ultrathin MXene multilayers. Hence, the surface possesses a self-cleaning ability to shed waterborne and oil-based liquids thanks to residue-free slipping motion. Passive anti-icing and active deicing capabilities are, respectively, obtained on the solar thermal surface, which effectively prevents water from freezing and simultaneously melts pre-formed ice and thick frost. The self-cleaning effect enables residue-free removal of unfrozen water and interfacially melted ice/frost to boost the anti-/deicing efficiency. Importantly, the surface is capable of self-healing under illumination to repair physical damage and chemical degradation.

1. Introduction

Ice buildup is ubiquitous in nature and engineering applications, which however can cause a catastrophic impact on a wide range of systems, including architectural windows, automobile windshields, overhead powerlines, solar panels, wind turbines, and aircraft wings.[1–4] There is a tremendous expenditure of manpower and material resources in ice removal worldwide every year.[4–20] A typical example is that the market of ice-protection systems was estimated to reach $20.04 billion by 2027.[21] Solar anti-/deicing based on photothermal materials is one of the most economically efficient and environmentally friendly methods to combat the icing problem, by converting sunlight into heat to prevent ice formation or melt the pre-formed ice.[22–36] However, photothermal materials are by nature, lightproof and appear black, because high optical absorption is an innate prerequisite for photothermal materials.[37–44] Hence, there intrinsically exists a mutually exclusive problem for solar anti-/deicing surfaces, between generating heat and retaining transparency at the fundamental level. However, it is unquestionable that transparency is highly desirable and, in many cases, essential for anti-/deicing surfaces, such as the architectural windows, automobile windshields, photovoltaics, aircraft coatings, and so forth. Besides, it is critically important to implement the photothermal anti-/deicing process under sunlight illumination, since near-infrared irradiation or illumination >1.0 sun is scarcely available under natural conditions.[25–29,45] Unfortunately, to the best of our knowledge, transparent photothermal anti-/deicing surfaces that can function under 1.0 sun illumination have never been reported, because of the formidable challenge to unify transparency and solar thermal properties. A related report by Poulikakos and co-workers demonstrated a photothermal anti-/deicing surface that works under 2.4 sun (2.4 kW m^{-2}) illumination and exhibits visible light transmittance of ≈36%.[26] In addition to lack of transparency, the solar anti-/deicing surfaces tailored for outdoor applications are prone to be smudged by various contaminants, physically damaged, and oxidized by ultraviolet radiation from the sun. Therefore, it is also highly desirable to

W. Niu, X. Liu, J. Sun
State Key Laboratory of Supramolecular Structure and Materials
College of Chemistry
Jilin University
Changchun 130012, China
E-mail: xiaokongliu@jlu.edu.cn
G. Y. Chen
Guangdong and Hong Kong Joint Research Centre for Optical Fiber Sensors
Shenzhen University
Shenzhen 518060, China
H. Xu
Future Industries Institute
University of South Australia
Mawson Lakes, South Australia 5095, Australia
The ORCID identification number(s) for the author(s) of this article can be found under https://doi.org/10.1002/adma.202108232.

DOI: 10.1002/adma.202108232

 © 2022 Wiley-VCH GmbH

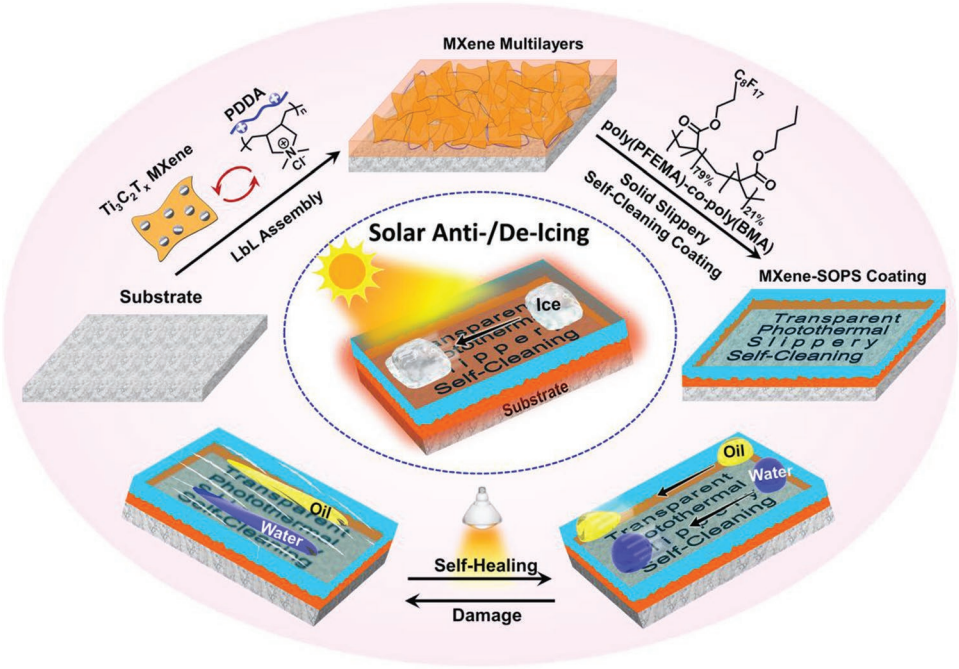

Scheme 1. Schematic illustration of the fabrication process, and the solar anti-/deicing, self-cleaning, and self-healing properties of the highly transparent photothermal coating.

endow solar anti-/deicing surfaces with self-cleaning and self-healing capabilities to lower their maintenance cost and extend their service life.

Dispersion of photothermal materials in water-repellent coatings, including superhydrophobic and liquid-infused slippery coatings, can generate photothermal anti-/deicing surfaces capable of shedding the unfrozen/melted water.[23,27–30,32–34] Such a wetting behavior keeps the surface free of water residues to avoid refreezing of the melted water. Nevertheless, transparency is extremely difficult to achieve in these kinds of photothermal anti-/deicing surfaces. The dispersed black photothermal materials significantly obstruct light transmission, while the light scattering effect of superhydrophobic and liquid-infused slippery coatings intrinsically suppress transparency due to their fractal and multi-phase structures, respectively.[23,27–30,32–34] Herein, we report a different concept for the fabrication of a self-healable solar anti-/deicing surface with high transparency and purposely engineered dewettability, by depositing a novel solid (i.e., liquid-free) omniphobic slippery (SOPS) coating onto layer-by-layer (LbL)-assembled ultrathin MXene multilayers (**Scheme 1**). The LbL-assembly technique, which is made advantageous by its simplicity and scalability,[46–49] enables precise control of the thickness of the MXene multilayers at the nanometer scale. Meanwhile, MXene is a perfect photothermal material reported to exhibit nearly 100% internal photothermal conversion efficiency.[50–53] With the above-described two qualities combined, the ideal MXene multilayer coatings are obtainable with high transparency and adequate photothermal performance for solar anti-/deicing purposes. A SOPS coating was further applied onto the MXene multilayers, via the solvent-free blade coating method, to reach the highly transparent solar anti-/deicing surface that enables efficient residue-free shedding of the unfrozen water and interfacially melted ice/frost. Taking the advantages of substrate-independence and scalability of both the LbL assembly and solvent-free blade coating techniques, the solar anti-/deicing surface is applicable to a large class of substrates with large areas.

Strikingly, the as-developed solar anti-/deicing surface enables the coated glass to exhibit transmittance >77% at 550 nm, while the photothermal property gives rise to a surface temperature increase by 31 °C under 1.0 sun illumination when the environmental temperature is as low as −30 °C. Therefore, such a solar thermal performance can effectively prevent water from freezing and melt pre-formed ice as well as frost in the most common cold environments. Remarkably, the omniphobic slippery anti-/deicing surface exhibits self-cleaning capability against waterborne and oil contamination, thanks to residue-free slipping motion of water and a wide range of organic liquids (Scheme 1), including liquids with surface tension spanning from 17.9 to 76.4 mN m^{-1}, strong acids and alkalis, and highly viscous liquids (e.g., glycerol with viscosity of 704 mPa s). Such a self-cleaning effect keeps the surface dry and clean, which is particularly suited for boosting the solar anti-/deicing effectiveness and efficiency. Importantly, the solar anti-/deicing surface can photothermally self-heal physical damage or chemical oxidation to restore its diminished self-cleaning ability (Scheme 1), due to heat-induced migration and reconfiguration of polymer chains, which is a convenient means to reduce the maintenance cost and extend the service life of the functional surface.

© 2022 Wiley-VCH GmbH

2. Results and Discussion

2.1. Preparation and Photothermal Property of the Anti-/Deeicing Surface

A typical type of MXene, $Ti_3C_2T_x$, reported to exhibit nearly 100% internal photothermal conversion efficiency,[51] was prepared and utilized as the photothermal material (see Experimental Section, Figures S1 and S2, Supporting Information). The MXene nanosheet with a thickness of ≈3.2 nm exhibits a typical two-dimensional lamellar structure with a large lateral size up to several micrometers (**Figure 1**a and Figure S3, Supporting Information). Such a high aspect ratio and low thickness of the MXene nanosheet facilitate the fabrication of transparent MXene multilayers by precisely controlling their overall thickness. Even the ultra-dilute MXene aqueous suspension (5 ppm) appears black and exhibits noticeable absorption in the UV–vis spectrum ranging from 300 to 900 nm with a characteristic absorption peak around 760 nm (Figure 1b). These results validate the outstanding solar absorption property of the MXene nanosheets, which is a prerequisite for harvesting solar energy to generate heat. MXene multilayers were fabricated by the LbL assembly technique, involving alternate deposition of the positively charged poly(diallyldimethylammonium) (PDDA) and negatively charged MXene nanosheets onto solid substrates. Taking advantage of the LbL assembly technique that is compatible with different substrates, the $(PDDA/MXene)_n$ multilayers with varied numbers of deposited bilayers (n) can be successfully fabricated onto virtually all kinds of water-insoluble substrates, including glass, silicon, ceramics, metals, plastics,

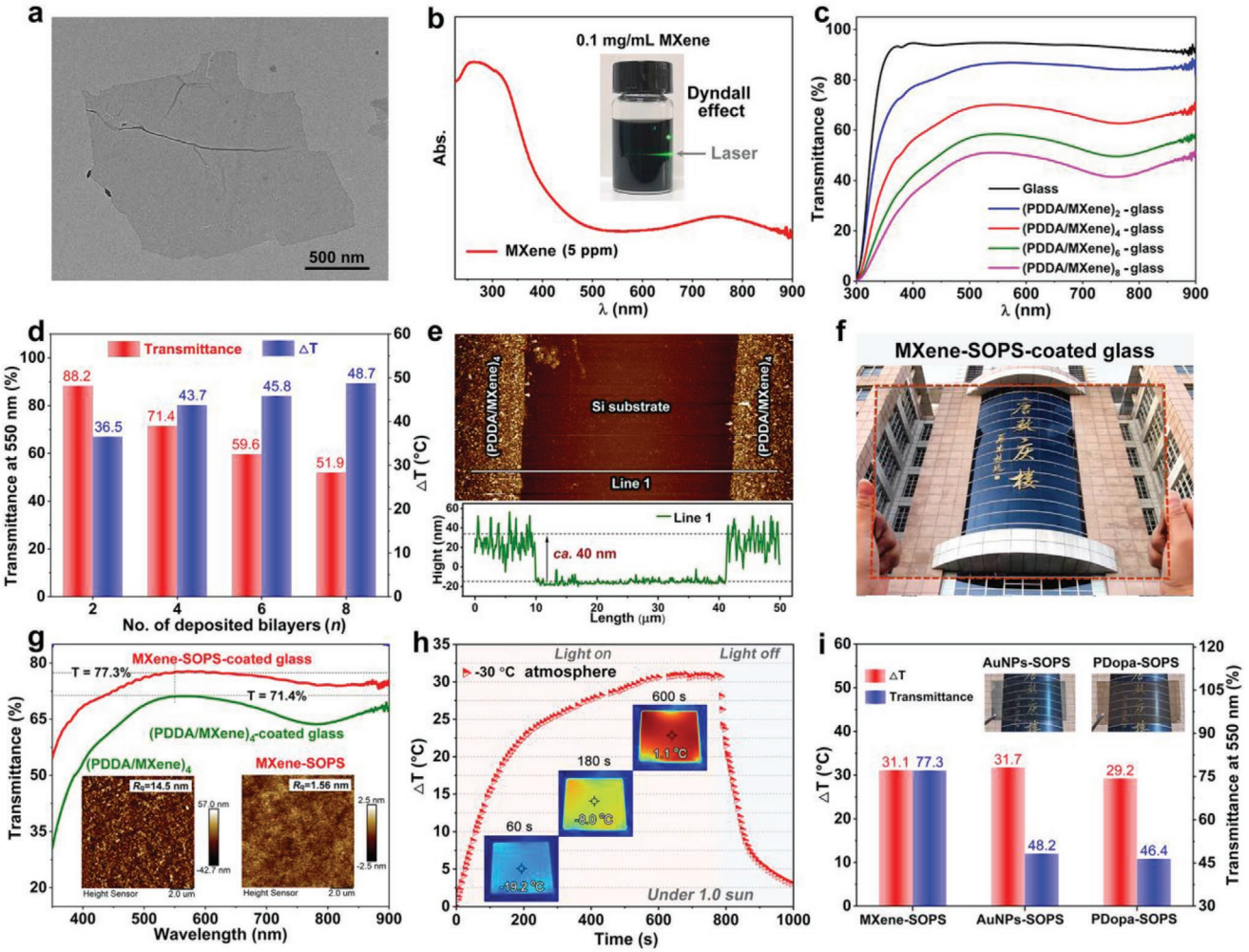

Figure 1. a) TEM image of the single-layered MXene ($Ti_3C_2T_x$) nanosheet. b) UV–vis absorption spectrum and Tyndall effect image of the aqueous suspensions of the MXene nanosheets. c) UV–vis transmission spectra of bare glass and the $(PDDA/MXene)_n$-coated glass with "n" varied from 2.0, 4.0, 6.0, to 8.0. d) Transmittance at 550 nm and photothermal temperature increase (ΔT, under 1.0 sun illumination, atmospheric temperature of 25 °C) of the $(PDDA/MXene)_n$-coated glass. e) Atomic force microscopy (AFM) image of the scratched $(PDDA/MXene)_4$ multilayers deposited on a Si substrate and the corresponding height profile along the line, the scratch is made to expose the substrate and determine the thickness of the MXene multilayers. f) Photograph of a piece of the MXene-SOPS-coated glass (32 × 20 cm^2). g) UV–vis transmission spectra of the $(PDDA/MXene)_4$- and MXene-SOPS-coated glass. Insets: AFM images of the $(PDDA/MXene)_4$ and MXene-SOPS coatings deposited on Si substrates. h) Time-dependent temperature increase of the MXene-SOPS-coated glass surface under 1.0 sun illumination at the atmospheric temperature of −30 °C. i) Comparison of transmittance and ΔT of the MXene-SOPS-, AuNPs-SOPS- and PDopa-SOPS-coated glass. Insets: Photographs of the AuNPs-SOPS- and PDopa-SOPS-coated glass.

© 2022 Wiley-VCH GmbH

and so forth. With the increase of the number of deposited bilayers, the transmittance of the $(PDDA/MXene)_n$-coated glass gradually decreases in the visible light regime (≈400–780 nm, Figure 1c), due to the increase of the light absorption by the MXene multilayers with increased thickness (Figure S4, Supporting Information). However, even the $(PDDA/MXene)_8$-coated glass is still visibly transparent with transmittance of 51.9% at 550 nm, despite the black nature of MXene. Encouragingly, the glass slide coated with $(PDDA/MXene)_4$ exhibits very high transparency, evidenced by the high transmittance of 71.4% at 550 nm (Figure 1c and Figure S5, Supporting Information). Photothermal performance of the MXene multilayers is verified by the fact that the surface temperature of the $(PDDA/MXene)_n$-coated glass rapidly rises and reaches the plateaus after 10-min illumination under 1.0 sun (1 kW m^{-2}) in the ambient atmosphere (Figure S6, Supporting Information). Figure 1d shows that the temperature increase (ΔT) of the $(PDDA/MXene)_n$-coated glass increases with the increase of the number of deposited bilayers (n), while the transparency of the samples follows the opposite trend. Notably, the $(PDDA/MXene)_4$-coated glass unifies high transparency and outstanding photothermal performance that gives rise to a ΔT of 43.7 °C under 1.0 sun illumination. Therefore, the ultrathin $(PDDA/MXene)_4$ multilayers with a thickness of ≈40 nm (Figure 1e) were exclusively employed as the solar thermal component of the anti-/deicing surface.

Self-cleaning capability was further conferred on the photothermal MXene multilayers by applying a novel SOPS coating derived from a deliberately designed low-surface-energy polymer, synthesized via the free-radical copolymerization of 2-(perfluorooctyl) ethyl methacrylate (PFEMA) and n-butyl methacrylate (BMA) (Figures S7 and S8, Supporting Information). The poly(PFEMA)-*co*-poly(BMA) copolymer (PFEMA:BMA = 3.7:1.0, molar ratio) as a crystalline thermoplastic exhibits a melting temperature (T_m) of 76.5 °C and a high decomposition temperature (T_d) of 268 °C (Figure S9, Supporting Information). The moderate melting temperature enables easy deposition of the copolymer onto a large class of substrates via the solvent-free blade coating technique (see Experimental Section in Supporting Information). Taking the $(PDDA/MXene)_4$-coated glass as an example, the melted poly(PFEMA)-*co*-poly(BMA) copolymer can be blade-coated onto the substrate to generate a 10 µm-thick MXene-SOPS composite coating (Figure S10, Supporting Information). Figure 1f shows that a large piece of MXene-SOPS-coated glass (32 × 20 cm^2) exhibits high transparency with negligible visibility fading. Compared to the glass solely coated with the MXene multilayers, the MXene-SOPS-coated glass shows significantly enhanced transparency with transmittance as high as 77.3% at 550 nm (T_{550nm}, Figure 1g), resulting from the reduced light absorption due to the lowered surface roughness (root mean square roughness, R_q, from 14.5 to 1.56 nm) (Figure 1g and Figures S11 and S12, Supporting Information). The highly transparent MXene-SOPS coating still exhibits excellent solar thermal performance, though the illumination-induced temperature increase, to some extent, decreases owing to decreased light absorption, compared to the MXene multilayers (Figure S12, Supporting Information). The surface temperature of the MXene-SOPS-coated glass rapidly rises and reaches a plateau with ΔT of ≈31 °C under 1.0 sun illumination for 10 min, independent of whether the ambient temperature is −30 or 25 °C (Figure 1h and Figure S13, Supporting Information). Crucially, the SOPS coating drastically enhances the stability of the underlying MXene, while unprotected MXene can be gradually oxidized in the presence of oxygen and water/moisture.[54] Note that the MXene-SOPS-coated glass shows little change after storage in the ambient atmosphere for more than one year. On the contrary, without SOPS-coating protection, the $(PDDA/MXene)_4$ multilayers degrade and become cloudy white in appearance after only 3 months in storage (Figure S14, Supporting Information).

The transparency and solar thermal performance of the MXene-SOPS coating were further compared with its counterparts, prepared from the widely reported photothermal materials via the same coating method, including the plasmonic Au nanoparticles (AuNPs) and melanin-like poly(L-dopa) (PDopa) (see Experimental Section in Supporting Information).[55–58] The as-prepared control samples are denoted as AuNPs-SOPS and PDopa-SOPS, respectively. Remarkably, the MXene-SOPS-coated glass slide exhibits far higher transparency (T_{550nm} = 77.3%) compared to those coated with AuNPs-SOPS (T_{550nm} = 48.2%) and PDopa-SOPS (T_{550nm} = 46.4%), while the three samples exhibit similar solar thermal performances with ΔT of ≈30°C (Figure 1i and Figure S15, Supporting Information). Due to the much lower transparency, the AuNPs-SOPS- and PDopa-SOPS-coated glass exhibits significant hindrance in visibility (inset of Figure 1i). On the one hand, the far superior solar thermal performance of the MXene-SOPS coating benefits from the outstanding light-to-heat conversion efficiency of MXene.[51] On the other hand, the LbL assembly is crucial to endow the MXene multilayers with an ultrathin and compact structure, which is a prerequisite for the high transparency of the MXene-SOPS coating.

2.2. Self-Cleaning Property of the MXene-SOPS Coating

The surface wettability and dewettability of the MXene-SOPS coating were, respectively, assessed by measuring the contact angles (CAs for 4 µL droplets) and sliding angles (SAs, tilting angles (TAs) required for the motion of 10 µL droplets) of a wide range of probe liquids, including water and organic liquids (e.g., ethanol and various oil). The CAs of the probe liquids increase with the increase of liquid surface tension (**Figure 2**a and Table S1, Supporting Information), while water with the highest surface tension (72.0 mN m^{-1}) exhibits a CA of ≈120° which is much smaller than that on a superhydrophobic surface (>150°). Nevertheless, water and the various organic liquids undergo slipping motion on the MXene-SOPS surface at low SAs, without leaving any residual traces behind (inset of Figure 2b). Although the SAs increase with increasing surface tension and viscosity of the liquids (Figure 2b and Table S1, Supporting Information), the high-surface-tension water and highly viscous glycerol (viscosity, 704 mPa s) still exhibit SAs as low as ≈25° and ≈24°, respectively. Encouragingly, n-hexane with an ultralow surface tension of 17.9 mN m^{-1} can slide down the MXene-SOPS surface, in residue-free manner, at a SA of only ≈8° (inset of Figure 2b). Therefore, the MXene-SOPS coating has an omniphobic slippery surface with excellent

© 2022 Wiley-VCH GmbH

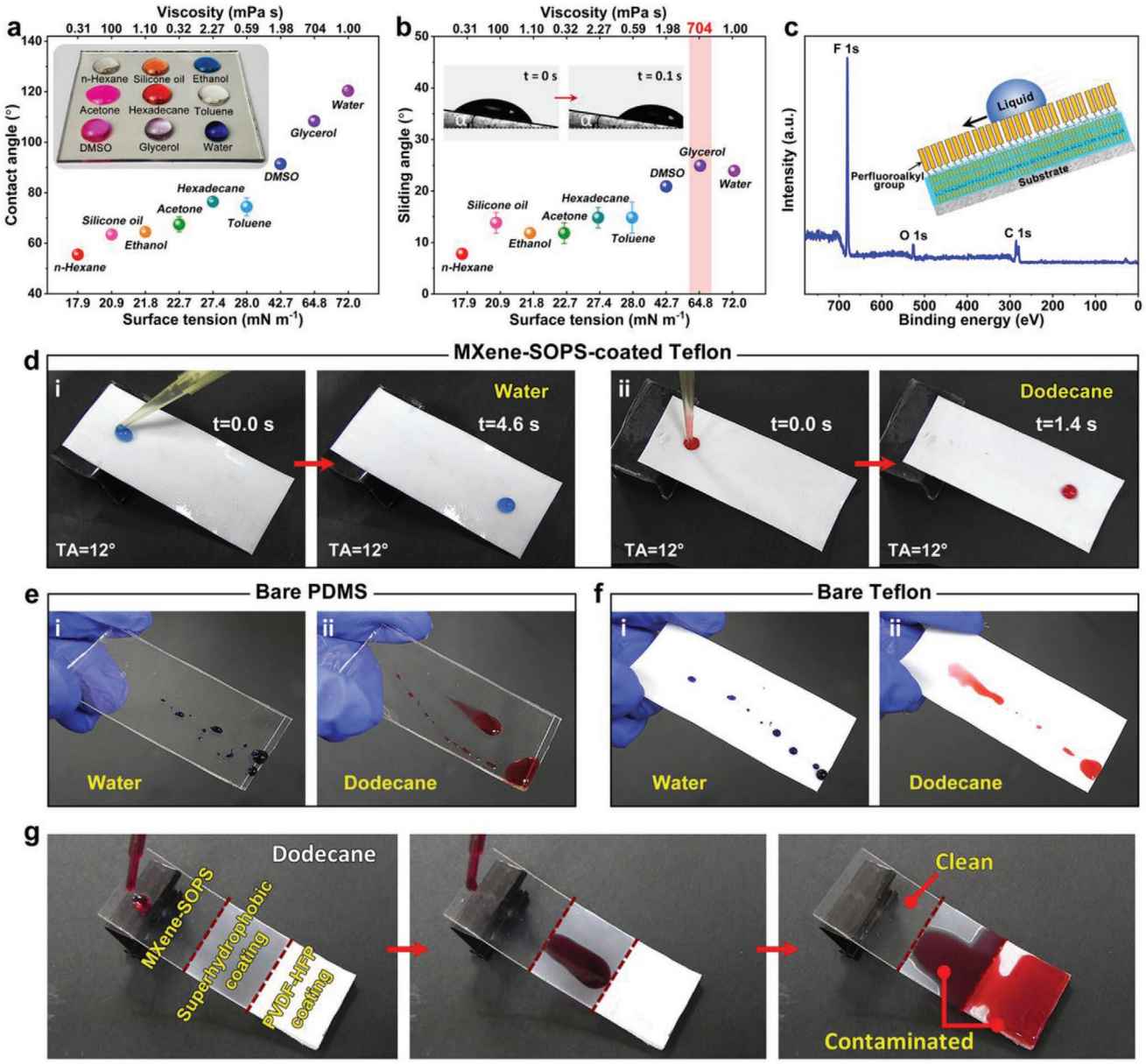

Figure 2. a,b) CAs (4 µL droplets (a)), SAs (10 µL droplets (b)) and photograph (inset of (a)) of various liquid droplets on the MXene-SOPS-coated glass surface. Inset of (b): Time-lapse snapshots of a sliding 10 µL n-hexane droplet on the MXene-SOPS-coated glass at a SA of 8.3°. c) XPS widescan spectrum of the MXene-SOPS coating. Inset: Schematic illustration of the perfluoroalkyl side groups that crystallize in a highly ordered, liquid crystalline smectic B phase. d–f) Snapshots taken when sliding the labeled water (30 µL (d_i,e_i,f_i)) and n-dodecane (30 µL (d_{ii},e_{ii},f_{ii})) droplets on the following samples: MXene-SOPS-coated Teflon (d), bare PDMS (e), and bare Teflon (f). g) Time-lapse snapshots taken during the sliding of labeled n-dodecane on the MXene-SOPS, superhydrophobic, and PVDF-HFP coatings.

dynamic dewettability.[59] The residue-free slipping motion of both water and oil makes the MXene-SOPS surface self-cleaning against waterborne and oil contamination. In this scenario, the MXene-SOPS coating offers an alternative of superomniphobic/superoleophobic coatings that repel both water and oil by suspending the liquid droplets with CA > 150°.[60–65] However, compared to the superhydrophobic coating that can repel only water, the superomniphobic/superoleophobic coating is very challenging to fabricate in practice and always appear opaque, due to the requirement of special surface textures with reentrant geometry or convex curvature.[60–65] X-ray photoelectron spectroscopy (XPS) measurement of the MXene-SOPS coating indicates that the atomic ratio between fluorine, oxygen, and carbon is 9.3:1.0:6.4 at the surface (Figure 2c). The very high atomic ratio between fluorine and oxygen signifies the enrichment of the perfluoroalkyl side groups on the coating surface. Previous studies have revealed that the perfluoroalkyl side groups with more than eight $-CF_2-$ units have a strong tendency to crystallize in a highly ordered, liquid crystalline smectic B phase.[66,67] The X-ray diffraction (XRD) measurement

© 2022 Wiley-VCH GmbH

of our SOPS coating verifies that the perfluoroalkyl side groups of the poly(PFEMA)-*co*-poly(BMA) copolymer indeed organize into the crystalline smectic B structure (Figure S16, Supporting Information). In this scenario, the $-CF_3$ end groups are uniformly arranged on the MXene-SOPS surface in a hexagonally organized layer (inset of Figure 2c).[67] Such a structural feature, to the fullest extent, lowers the surface free energy and screens the electrical effect of the polar groups.[68] As a result, the interactions between the surface and different contacting liquids are drastically diminished, endowing the MXene-SOPS coating with an omniphobic slippery surface possessing self-cleaning capability against waterborne and oil contamination.

Thanks to the advantage of the LbL assembly and solvent-free blade coating techniques that feature scalable applicability to a large class of substrates, the MXene-SOPS coating can be fabricated onto glass, ceramic, metals, and plastics to endow them with self-cleaning capability. Figure 2d and Figure S17a, Supporting Information, show that the labeled water and oil (exampled by n-dodecane) droplets readily slide down the tilted MXene-SOPS-coated Teflon and glass, respectively, without leaving any trace behind (Movies S1 and S2, Supporting Information). In sharp contrast, both water and oil spread on the hydrophilic $(PDDA/MXene)_4$ surfaces, making them severely contaminated (Figure S17b and Movies S1 and S2, Supporting Information). The typical low-surface-energy materials, poly(dimethylsiloxane) (PDMS) and Teflon, were also taken for comparison. Notably, both water and oil leave considerable residual traces along the traveled paths when sliding down the bare PDMS and Teflon surfaces (Figure 2e,f and Movies S1 and S2, Supporting Information), though Teflon is regarded as the benchmark nonstick material that is widely available. All these results confirmatively reveal that the MXene-SOPS coating has a special omniphobic slippery surface, making it self-cleaning against both waterborne and oil contamination. In terms of the resistance of waterborne contamination, the MXene-SOPS coating is similar to a superhydrophobic surface (Figure S18 and Movie S3, Supporting Information), despite the higher water sliding angle compared to that on a superhydrophobic surface. However, oil can aggressively wet/contaminate the superhydrophobic coating and also the plain hydrophobic coating prepared from the commercial fluorinated copolymer of PVDF-HFP (Figure 2g and Movie S3, Supporting Information). In sharp contrast, the MXene-SOPS coating can also effectively resist oil contamination thanks to the residue-free slipping motion of oil droplets (Figure 2g and Movie S3, Supporting Information). It is worth noting that preparation of the MXene-SOPS coating just involves aqueous dip-coating and solvent-free blade coating procedures, while the previously reported SOPS coatings were always fabricated from organic solvents (e.g., tetrahydrofuran, acetonitrile, toluene, isopropanol).[69–74] Therefore, production of the MXene-SOPS coating is environmentally friendly with minimal toxicity, making it applicable to the solvent-sensitive substrates, such as polystyrene that can be dissolved by many organic solvents (Figure S19, Supporting Information).

To further demonstrate the self-cleaning effect of the MXene-SOPS coating toward different liquids, **Figure 3**a shows that a broad range of labeled droplets, including water, dimethyl sulfoxide (DMSO), ethanol, silicone oil, glycerol, and strong acid (3 M HCl) and alkali (3M NaOH), can spontaneously slide down the highly transparent MXene-SOPS-coated glass (32×20 cm^2) at a TA of ≈20° without leaving a trace behind (Movie S4, Supporting Information). Strikingly, a ceramic bowl with the transparent MXene-SOPS coating exhibits excellent self-cleaning performance even against the contamination of the highly viscous glycerol (Figure 3b). The self-cleaning effect of the MXene-SOPS coating enables the coated substrates to easily remove dust by water rinsing and exhibit anti-smudge properties for anti-graffiti and anti-fingerprint applications (Figure 3c and Figure S20, Supporting Information). Furthermore, the MXene-SOPS coating can work as a chemical barrier to protect plastics (e.g., polystyrene) or metals (e.g., aluminum) from dissolution or corrosion by organic solvents or acids/alkalis, respectively, owing to the chemically inert nature of the SOPS coating and its dynamic dewettability toward liquids (Figures S19 and S21, Supporting Information). Importantly, the MXene-SOPS coating has high adhesion to both rigid (e.g., glass, adhesion rating of 5B, ASTM D3359 tape tests, Figure S22, Supporting Information) and flexible (e.g., polyimide, PI) substrates to maximize endurance for practical applications. In the case of MXene-SOPS-coated flexible PI sheet, after 1000 times of twist followed by multiple folds, no delamination or damage of the coating was observed. The silicone oil can still slide down the twisted and folded PI surface without leaving any trace behind, even along the creases generated by the folding treatments (Figure S23 and Movie S5, Supporting Information). Furthermore, the sand abrasion and water-flushing tests indicate that the MXene-SOPS coating possesses satisfactory mechanical robustness to withstand the most common mechanical wear in practical applications (Figure S24, Supporting Information).[63] The abrasion resistance of the MXene-SOPS coating was quantitatively measured to be 339 L mil^{-1}, following the ASTM-D968 standard falling sand abrasion test (Figure S25, Supporting Information). Additionally, the MXene-SOPS coating can even tolerate 300 cycles of heating and freezing treatments (60 °C and −30 °C for 12 h, Figure S26, Supporting Information), suggesting high tolerance to extreme weather conditions.

To demonstrate the scalability of the MXene-SOPS coating, the meter-scale commercial poly(ethylene terephthalate) (PET) films (e.g., window films) were coated, resulting in affixable films with self-cleaning and solar thermal properties. The highly transparent MXene-SOPS-coated PET film (Figure S27, Supporting Information) can be applied onto a large piece of glass (1.2×1.0 m^2) to endow the covered area (1.0×0.6 m^2) with self-cleaning capability to shield against the waterborne and oil contamination (Figure 3d,e and Movie S6, Supporting Information). The MXene-SOPS-coated PET film also exhibits excellent solar thermal performance that enables the surface temperature to increase by ≈31 °C under 1.0 sun illumination (Figure 3f). Therefore, the MXene-SOPS-coated PET film can be further applied onto other substrates that are difficult to readily coat (e.g., architectural windows and automobile windshields) for solar anti-/deicing and self-cleaning purposes. Taken together, as summarized in Figure 3g, the highly transparent photothermal MXene-SOPS coating possesses a number of beneficial features for practical anti-/deicing applications. Importantly, the self-cleaning property not only enables residue-free shedding of unfrozen water and interfacially melted ice/frost from the photothermally heated surface but also keeps

© 2022 Wiley-VCH GmbH

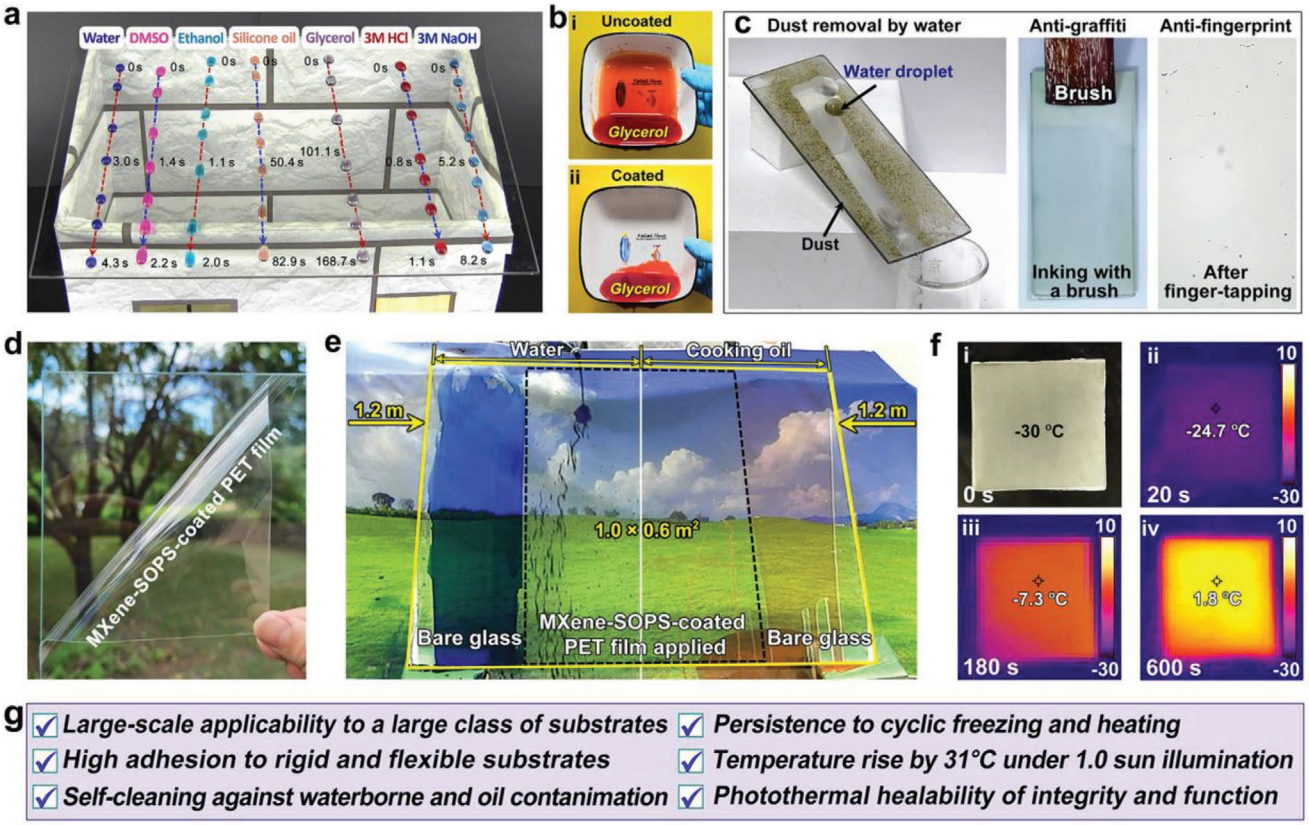

Figure 3. a) Synthetic image generated by overlapping the time-lapse snapshots taken when sliding the various labeled droplets on the MXene-SOPS-coated glass, the sliding times of the liquids are provided in the image. b) Snapshots taken when flowing the labeled glycerol in the pristine (i) and MXene-SOPS-coated (ii) ceramic bowls. c) Photographs (left and middle images) and microscopy image (right image) showing self-cleaning effect (i.e., dust removal by water droplets, left image), anti-graffiti (middle image), and anti-fingerprint (right image) properties of the MXene-SOPS-coated glass. d) Photograph of the MXene-SOPS-coated PET affixable film applied on glass. e) Snapshots taken when pouring labeled water and cooking oil on bare glass and glass covered by the MXene-SOPS-coated PET film. f) Photograph (i) and infrared thermal images (ii–iv) of the MXene-SOPS-coated PET film after 1.0 sun illumination for different times at the atmospheric temperature of −30 °C. g) Summary of the beneficial features of the MXene-SOPS coating.

the surface clean and dry to boost the anti-/deicing efficiency and retain high light-to-heat conversion efficiency. Furthermore, the material cost for the industrial production of the MXene-SOPS coating is estimated to be as low as ≈4.1 $ per m^2, since only small amounts of raw materials, are required for the production of the functional coating (see details in Table S2, Supporting Information).

2.3. Solar Anti-/Deicing Performance of the MXene-SOPS Coating

Taking the MXene-SOPS-coated glass as an example, the photothermal anti-/deicing performance was studied under 1.0 sun illumination in a custom-built freezer chamber with an environmental temperature of −25 °C. The passive anti-icing property was first tested by placing the sample on a piece of foam board (i.e., insulation layer, TA of 20°) at the bottom of the chamber (**Figure** 4$a_{i,ii}$). After 1.0 sun illumination for 10 min, the surface temperature of the samples rises to ≈6 °C (Figure 4b_i,c_i), followed by challenging the samples by supercooled water droplets (0 °C, Figure 4a_i) or room-temperature water mist generated by a humidifier (Figure 4a_{ii}). The water droplets quickly slide down the photothermally heated surface to leave the surface clean and dry (Figure 4$b_{ii–iv}$), while the water mist condensed on the surface gradually accumulates into water droplets that can continuously slide down the surface to leave the surface clean as well (Figure 4$c_{ii–iv}$ and Movie S7, Supporting Information). Controlled experiments were conducted on the following samples: i) bare glass without photothermal or self-cleaning properties, ii) self-cleaning SOPS-coated glass without photothermal property, iii) photothermal $(PDDA/MXene)_4$-coated glass without self-cleaning property. As expected, ice quickly forms on the bare glass surface when being affected by water droplets or water mist (Figures S28a and S29a, Supporting Information). Although the self-cleaning SOPS-coated glass, to some extent, delays the icing process because of the surface dewettability, ice formation eventually occurs on the surface with a constant influx of water droplets or water mist (Figures S28b and S29b, Supporting Information). Ice formation is suppressed on the photothermal $(PDDA/MXene)_4$-coated glass, but the unfrozen water remains on the surface, which refreezes in the absence of illumination (Figures S28c and S29c and Movie S7, Supporting Information). Subsequently, the active deicing property of the

© 2022 Wiley-VCH GmbH

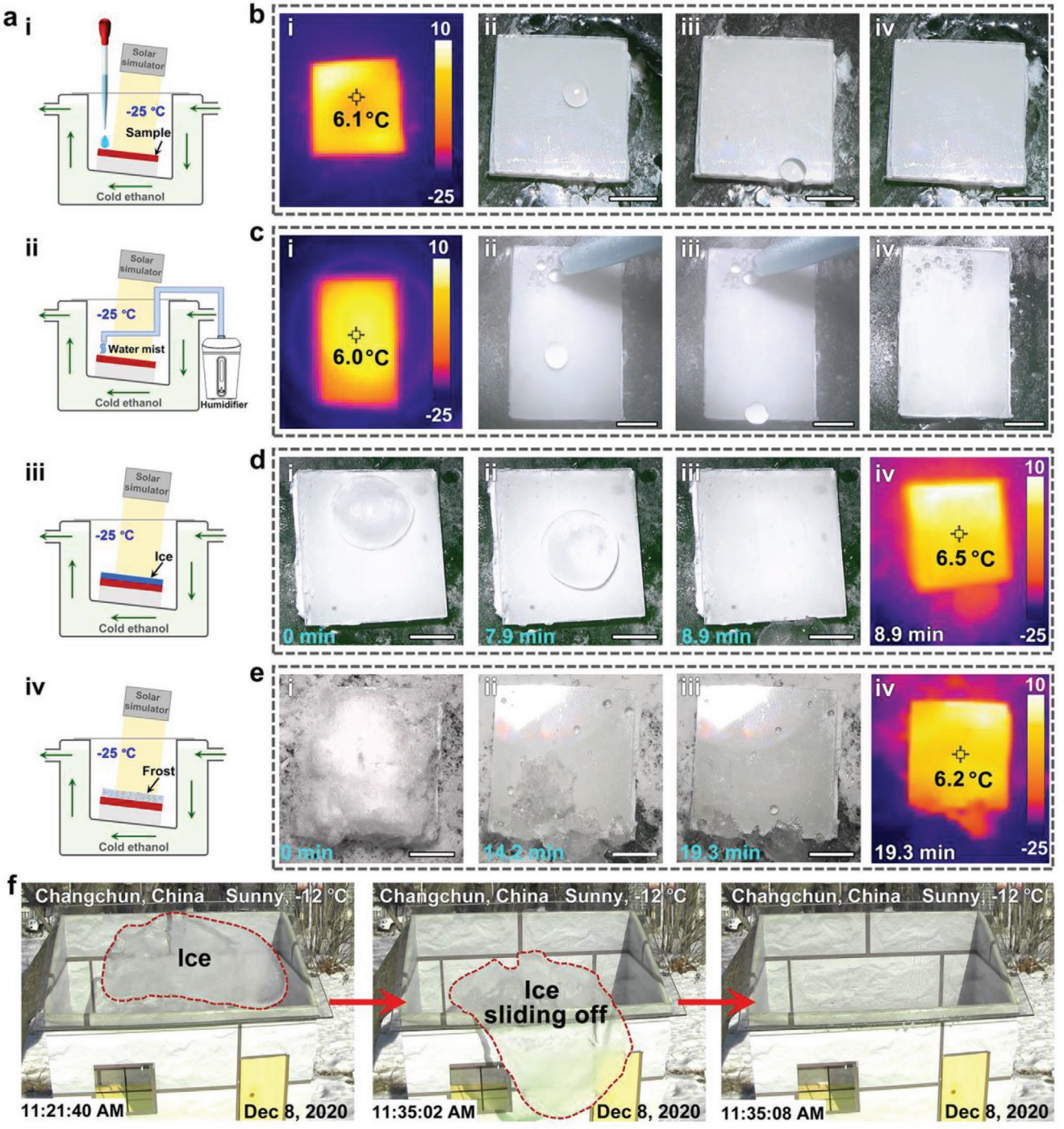

Figure 4. a) Schematic illustration of the apparatuses used for the anti-icing ((a_i) for water droplets, (a_{ii}) for water mist), deicing (a_{iii}), and de-frosting (a_{iv}) experiments. b,c) Infrared thermal images of the MXene-SOPS-coated glass after being illuminated under 1.0 sun for 10 min (i), and sequential images (ii–iv) taken when challenging the samples by water droplets (b) and water mist (c) under 1.0 sun illumination. d,e) Time-lapse snapshots taken during the deicing (d) and de-frosting (e) processes on the MXene-SOPS-coated glass under 1.0 sun illumination (i–iii), and infrared thermal images of the samples after the removal of ice and frost (iv). The atmospheric temperature for all the above-described experiments is –25 °C. The scale bars are 10 mm. f) Time-lapse snapshots taken during the solar deicing process on the MXene-SOPS-coated glass (32 × 20 cm^2), conducted in an outdoor environment with temperature of –12 °C.

MXene-SOPS-coated glass was tested by using the samples, on which ice or frost is formed prior to the 1.0 sun illumination (Figure 4$a_{iii,iv}$). As shown in Figure 4d and Movie S7, Supporting Information, the whole piece of quasi-hemispherically shaped ice quickly slides down the surface after 1.0 sun illumination for 8 min due to the melting of the ice at the coating–ice

© 2022 Wiley-VCH GmbH

interface, leaving a clean and dry surface with temperature of ≈6.5 °C. This phenomenon verifies that the dynamic dewetting (i.e., self-cleaning) capability of the MXene-SOPS coating effectively boosts the photothermal deicing efficiency without the need to melt the entire block of ice. Compared to ice, frost is more challenging to melt under illumination, because frost strongly reflects and scatters light due to its fractal and porous structure. Encouragingly, the thick layer of frost (≈0.5 cm thick), pre-formed on the MXene-SOPS-coated glass, gradually melts, shrinks, and then quickly slides down the surface under 1.0 sun illumination within 20 min (Figure 4e and Movie S7, Supporting Information). In sharp contrast, ice or frost on the bare glass and self-cleaning SOPS-coated glass does not show any change even after elongated 1.0 sun illumination for 2 h (Figures S30a,b and S31a,b, Supporting Information). Although the $(PDDA/MXene)_4$-coated glass can melt ice and frost into water under illumination, water residue cannot be properly removed from the surface and thus refreezes without continuous illumination (Figures S30c and S31c, Supporting Information). Therefore, the photothermal property of the MXene multilayers and the self-cleaning effect of the SOPS coating are both prerequisites for the effective and efficient anti-/deicing applications. To practically assess the deicing capability of the highly transparent MXene-SOPS coating, a piece of MXene-SOPS-coated glass (32×20 cm^2) adhered with a pre-formed ice layer (≈0.6 cm thick) was subjected to an outdoor environment with temperature of –12 °C on a sunny day in the winter of Changchun, China (December 8th, 2020). It was observed that the ice started to melt at the coating–ice interface after exposure to sunlight for ≈15 min and the entire layer of ice quickly slid off the surface without water residue left (Figure 4f and Movie S8, Supporting Information), demonstrating the practical applicability of the solar anti-/deicing MXene-SOPS coating. It is worth noting that the smooth MXene-SOPS coating eliminates the interlocking effect between ice and the surface rough structures, which is a well-acknowledged problem for superhydrophobic anti-/deicing surfaces.[4,63,75–81] Moreover, the solid nature of the MXene-SOPS coating is expected to make it more stable and durable for real-world applications, compared to the anti-/deicing coatings with liquid-infused slippery surfaces.[27,82–85]

2.4. Photothermal Healability of the MXene-SOPS Coating

The photothermal property of the MXene-SOPS coating provides the coating surface with illumination-driven self-healing capability to restore its structural integrity from the physical damage or chemical degradation, maintaining maximum self-cleaning performance. **Figure 5**a shows that the surface temperature of the MXene-SOPS-coated glass rises to an equilibrium temperature of ≈77 °C from the original temperature of ≈25 °C, under 1.5 sun (1.5 kW m^{-2}) illumination for 10 min. Such an equilibrium temperature reaches the T_m (76.5 °C) of poly(PFEMA)-*co*-poly(BMA), rendering the polymer molten and making the polymer chains highly mobile. In this scenario, physical damage can be easily repaired via the self-healing process under illumination. As shown in Figure 5b, the scratches inflected by scraping with a piece of sandpaper, can be completely healed after 1.5 sun illumination for 2 h. The as-worn surface loses its self-cleaning property because the scratches significantly impede the motion of the droplet, showing that a considerable amount of residue is left along the sliding trace of a glycerol droplet (Figure 5c$_i$). In sharp contrast, the self-cleaning capability of the surface can be recovered after the healing process, manifested by the fact that the highly viscous glycerol droplet (20 µL) can again slide down the surface without leaving any trace behind at a TA of only 12° (Figure 5c$_{ii}$). Moreover, the lost self-cleaning performance, induced by oxidation, can also be healed under illumination. O_2-plasma etching for 5 min was employed to simulate the chemical oxidation of the MXene-SOPS coating. The O_2-plasma etching leads to oxidation of the surface and thus significantly increases its surface energy, resulting in spreading of the glycerol droplet on the plasma-etched sample (Figure 5d$_i$). XPS measurements reveal significant increase in the atomic ratio between oxygen and fluorine after the etching process (Figure 5e), accompanied by the distinct decrease of the glycerol contact angle from 108° to 82° (Figure 5f). The O_2-plasma-etched sample can easily restore its self-cleaning property after being illuminated under 1.5 sun for 30 min, reinstating the residue-free slipping motion of the glycerol droplet on the surface (Figure 5d$_{ii}$). The photothermal effect of the MXene-SOPS coating makes the polymer chains at the surface highly mobile at elevated temperatures. The migration of the polymer chains results in the self-segregation and enrichment of the perfluoroalkyl groups at the coating-air interface, thus recovering the surface chemistry of the coating (Figure 5e) and also the contact angle of the probe liquid (Figure 5f). Strikingly, the self-cleaning property of the MXene-SOPS coating can be healed after the cyclic etching–illumination process. The contact and sliding angles of the glycerol droplets hardly change even after 5 cycles of the etching–illumination process (Figure 5f). Note that the photothermally heated MXene-SOPS coating exhibits negligible fluidity within the time range of illumination, though the equilibrium temperature of the coating surface reaches the melting temperature of the polymer. This result can be explained by the fact that the molten poly(PFEMA)-*co*-poly(BMA) has an extremely high viscosity of 6.4×10^5 mPa s at 77.5 °C, measured at the shear rate of 1.0 s^{-1} (Figure S32, Supporting Information), while the molten polymer can be quickly solidified after the removal of illumination. Overall, the photothermal self-healing property of the MXene-SOPS coating can effectively lower the maintenance cost and significantly extend the service life of the anti-/deicing surface. Moreover, the photothermal self-healing process can be implemented by remote illumination in a localized area, making the repair of the coating surface convenient and practical.

3. Conclusion

We have surmounted the formidable challenge to unify transparency and photothermal properties in a solar anti-/deicing surface that functions under 1.0 sun illumination. The highly transparent and scalable solar anti-/deicing surface can be fabricated onto a large class of substrates (e.g., glass, ceramics, metals, and plastics), by applying a SOPS coating on top of LbL assembled ultrathin MXene multilayers.

© 2022 Wiley-VCH GmbH

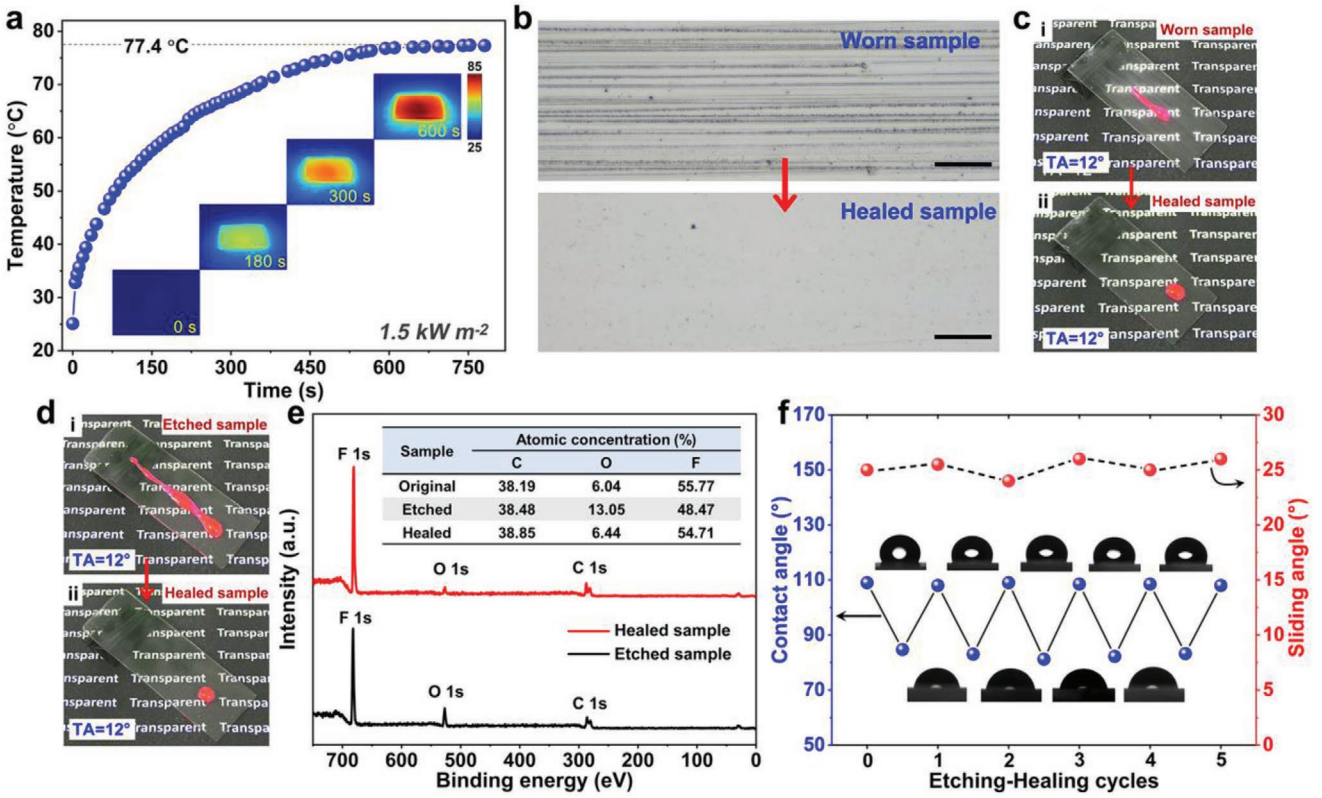

Figure 5. a) Time-dependent surface temperature of the MXene-SOPS-coated glass under 1.5 sun (1.5 kW m^{-2}) illumination at the atmospheric temperature of 25 °C. b) Microscopy images of the sandpaper-worn (upper image) and healed (under image) surfaces of the MXene-SOPS-coated glass, the scale bars are 50 µm. c,d) Snapshots taken when sliding the labeled glycerol droplets on the sandpaper-worn (c_i), O_2-plasma-etched (d_i), and healed (c_{ii},d_{ii}) surfaces of the MXene-SOPS-coated glass. e) XPS wide scan spectra of the O_2-plasma-etched and healed MXene-SOPS surfaces. f) CAs (4 µL) and SAs (10 µL) of glycerol droplets on the MXene-SOPS-coated glass surface after undergoing different cycles of etching-healing treatments.

The MXene-SOPS-coated glass exhibits high transparency with transmittance >77% at 550 nm, while the photothermal behavior elevates the surface temperature by 31 °C with respect to ambient under 1.0 sun illumination. Such a solar thermal effect enables the MXene-SOPS surface to passively anti-ice and actively deice, respectively, by effectively preventing water from freezing and efficiently melting the pre-formed ice/frost (e.g., 0.5 cm thick). The solar anti-/deicing surface also possesses omniphobic self-cleaning features to keep itself clean and dry, by spontaneously shedding various waterborne and organic liquids due to their residue-free slipping motion. Such a self-cleaning effect enables the surface to remove the unfrozen water and interfacially melted ice/frost in a timely manner without leaving water residue. In this scenario, the solar anti-/deicing effectiveness and efficiency can be significantly boosted and the light-to-heat conversion efficiency can be retained. Furthermore, deposition of the MXene-SOPS coating onto flexible PET films yields highly transparent affixable films with self-cleaning and photothermal properties. The resultant meter-scale affixable film can be conveniently applied onto other substrates (e.g., architectural windows and automobile windshields) to endow them with self-cleaning and solar anti-/deicing properties. Conveniently, the photothermal MXene-SOPS coating is capable of self-healing under illumination to repair physical damage and chemical degradation, enabling restoration of the lost self-cleaning property resulting from wear or oxidation. It is believed that the substrate-independent and self-healable MXene-SOPS coating, which has unprecedentedly achieved the feat of unifying high transparency and excellent solar thermal properties, will find a wide range of practical outdoor applications for anti-/deicing, self-cleaning, and anti-smudge purposes, in the fields of civil construction, automobile, power networks, photovoltaics, wind power, and aeronautics.

Supporting Information

Supporting Information is available from the Wiley Online Library or from the author.

Acknowledgements

X.L. thanks the National Key R&D Program of China (2018YFC1105401) for the financial support.

Conflict of Interest

The authors declare no conflict of interest.

© 2022 Wiley-VCH GmbH

Data Availability Statement

The data that support the findings of this study are available from the corresponding author upon reasonable request.

Keywords

anti-/deicing, coatings, layer-by-layer assembly, photothermal materials, self-healing materials

Received: October 13, 2021
Revised: December 8, 2021
Published online: January 28, 2022

[1] T. Bartels-Rausch, *Nature* **2013**, *494*, 27.
[2] R. W. Gent, N. P. Dart, J. T. Cansdale, *Philos. Trans. R. Soc., A* **2000**, *358*, 2873.
[3] O. Parent, A. Ilinca, *Cold Reg. Sci. Technol.* **2011**, *65*, 88.
[4] M. J. Kreder, J. Alvarenga, P. Kim, J. Aizenberg, *Nat. Rev. Mater.* **2016**, *1*, 15003.
[5] J. B. Boreyko, C. P. Collier, *ACS Nano* **2013**, *7*, 1618.
[6] J. Lv, Y. Song, L. Jiang, J. Wang, *ACS Nano* **2014**, *8*, 3152.
[7] Z. He, W. J. Xie, Z. Liu, G. Liu, Z. Wang, Y. Q. Gao, J. Wang, *Sci. Adv.* **2016**, *2*, e1600345.
[8] L. Wang, Q. Gong, S. Zhan, L. Jiang, Y. Zheng, *Adv. Mater.* **2016**, *28*, 7729.
[9] K. Golovin, S. P. Kobaku, D. H. Lee, E. T. DiLoreto, J. M. Mabry, A. Tuteja, *Sci. Adv.* **2016**, *2*, e1501496.
[10] S. Zhang, J. Huang, Y. Cheng, H. Yang, Z. Chen, Y. Lai, *Small* **2017**, *13*, 1701867.
[11] Q. Li, Z. Guo, *J. Mater. Chem. A* **2018**, *6*, 13549.
[12] C. C. M. Sproncken, R. Suris-Valls, H. E. Cingil, C. Detrembleur, I. K. Voets, *Macromol. Rapid Commun.* **2018**, *39*, 1700814.
[13] Y. Shen, Y. Wu, J. Tao, C. Zhu, H. Chen, Z. Wu, Y. Xie, *ACS Appl. Mater. Interfaces* **2018**, *11*, 3590.
[14] R. Chatterjee, D. Beysens, S. Anand, *Adv. Mater.* **2019**, *31*, 1807812.
[15] P. Irajizad, A. Al-Bayati, B. Eslami, T. Shafquat, M. Nazari, P. Jafari, V. Kashyap, A. Masoudi, D. Araya, H. Ghasemi, *Mater. Horiz.* **2019**, *6*, 758.
[16] K. Golovin, A. Dhyani, M. Thouless, A. Tuteja, *Science* **2019**, *364*, 371.
[17] Z. He, C. Wu, M. Hua, S. Wu, D. Wu, X. Zhu, J. Wang, X. He, *Matter* **2020**, *2*, 723.
[18] F. Wang, S. Xiao, Y. Zhuo, W. Ding, J. He, Z. Zhang, *Mater. Horiz.* **2019**, *6*, 2063.
[19] Y. Zhuo, J. Chen, S. Xiao, T. Li, F. Wang, J. He, Z. Zhang, *Mater. Horiz.* **2021**, *8*, 3266.
[20] S. Yang, C. Wu, G. Zhao, J. Sun, X. Yao, X. Ma, Z. Wang, *Cell Rep. Phys. Sci.* **2021**, *2*, 100474.
[21] *Global Full Ice Protection System (FIPS) Industry Research Report, Growth Trends and Competitive Analysis 2021–2027*, https://www.industryresearch.biz/global-full-ice-protection-system-fips-industry-18252586, (accessed: August, 2021).
[22] S. Dash, J. de Ruiter, K. K. Varanasi, *Sci. Adv.* **2018**, *4*, eaat0127.
[23] T. Cheng, R. He, Q. Zhang, X. Zhan, F. Chen, *J. Mater. Chem. A* **2015**, *3*, 21637.
[24] H. Guo, M. Liu, C. Xie, Y. Zhu, X. Sui, C. Wen, Q. Li, W. Zhao, J. Yang, L. Zhang, *Chem. Eng. J.* **2020**, *402*, 126161.
[25] G. Zhang, Q. Zhang, T. Cheng, X. Zhan, F. Chen, *Langmuir* **2018**, *34*, 4052.
[26] E. Mitridis, T. M. Schutzius, A. Sicher, C. U. Hail, H. Eghlidi, D. Poulikakos, *ACS Nano* **2018**, *12*, 7009.
[27] X. Yin, Y. Zhang, D. Wang, Z. Liu, Y. Liu, X. Pei, B. Yu, F. Zhou, *Adv. Funct. Mater.* **2015**, *25*, 4237.
[28] G. Jiang, L. Chen, S. Zhang, H. Huang, *ACS Appl. Mater. Interfaces* **2018**, *10*, 36505.
[29] L. Ma, J. Wang, F. Zhao, D. Wu, Y. Huang, D. Zhang, Z. Zhang, W. Fu, X. Li, Y. Fan, *Compos. Sci. Technol.* **2019**, *181*, 107696.
[30] S. Wu, Y. Du, Y. Alsaid, D. Wu, M. Hua, Y. Yan, B. Yao, Y. Ma, X. Zhu, X. He, *Proc. Natl. Acad. Sci. USA* **2020**, *117*, 11240.
[31] C. Wu, H. Geng, S. Tan, J. Lv, H. Wang, Z. He, J. Wang, *Mater. Horiz.* **2020**, *7*, 2097.
[32] Y. Liu, Y. Wu, Y. Liu, R. Xu, S. Liu, F. Zhou, *ACS Appl. Mater. Interfaces* **2020**, *12*, 46981.
[33] M. Wang, T. Yang, G. Cao, X. Wang, Z. Jiang, C. Wang, Y. Li, *Chem. Eng. J.* **2021**, *408*, 127316.
[34] W. Ma, Y. Li, C. Y. H. Chao, C. Y. Tso, B. Huang, W. Li, S. Yao, *Cell Rep. Phys. Sci.* **2021**, *2*, 100384.
[35] H. Zhang, G. Zhao, S. Wu, Y. Alsaid, W. Zhao, X. Yan, L. Liu, G. Zou, J. Lv, X. He, Z. He, J. Wang, *Proc. Natl. Acad. Sci. USA* **2021**, *118*, e2100978118.
[36] Z. Zhou, Q. Song, B. Huang, S. Feng, C. Lu, *ACS Nano* **2021**, *15*, 12405.
[37] H. Ghasemi, G. Ni, A. M. Marconnet, J. Loomis, S. Yerci, N. Miljkovic, G. Chen, *Nat. Commun.* **2014**, *5*, 4449.
[38] L. Zhang, B. Tang, J. Wu, R. Li, P. Wang, *Adv. Mater.* **2015**, *27*, 4889.
[39] M. Q. Yang, M. Gao, M. Hong, G. W. Ho, *Adv. Mater.* **2018**, *30*, 1802894.
[40] H. Qi, T. Wei, W. Zhao, B. Zhu, G. Liu, P. Wang, Z. Lin, X. Wang, X. Li, X. Zhang, J. Zhu, *Adv. Mater.* **2019**, *31*, 1903378.
[41] W. Wang, Y. Shi, C. Zhang, S. Hong, L. Shi, J. Chang, R. Li, Y. Jin, C. Ong, S. Zhuo, P. Wang, *Nat. Commun.* **2019**, *10*, 3012.
[42] C. Zhang, H. Q. Liang, Z. K. Xu, Z. Wang, *Adv. Sci.* **2019**, *6*, 1900883.
[43] Z.-Q. Li, Z.-Q. Wu, X.-L. Ding, M.-Y. Wu, X.-H. Xia, *CCS Chem.* **2021**, *3*, 2174.
[44] S. Mu, J. Nan, C. Shi, X. Tang, S. Liu, H. Chen, J. Zhang, B. Yang, *Macromol. Rapid Commun.* **2020**, *41*, 2000390.
[45] M. Meftah, L. Damé, D. Bolsée, A. Hauchecorne, N. Pereira, D. Sluse, G. Cessateur, A. Irbah, J. Bureau, M. Weber, K. Bramstedt, T. Hilbig, R. Thiéblemont, M. Marchand, F. Lefèvre, A. Sarkissian, S. Bekki, *Astron. Astrophys.* **2018**, *611*, A1.
[46] G. Decher, *Science* **1997**, *277*, 1232.
[47] L. Yu, G. Y. Chen, H. Xu, X. Liu, *ACS Nano* **2016**, *10*, 1076.
[48] H. An, T. Habib, S. Shah, H. Gao, M. Radovic, M. J. Green, J. L. Lutkenhaus, *Sci. Adv.* **2018**, *4*, eaaq0118.
[49] J. Lipton, G.-M. Weng, J. A. Röhr, H. Wang, A. D. Taylor, *Matter* **2020**, *2*, 1148.
[50] M. Naguib, M. Kurtoglu, V. Presser, J. Lu, J. Niu, M. Heon, L. Hultman, Y. Gogotsi, M. W. Barsoum, *Adv. Mater.* **2011**, *23*, 4248.
[51] R. Li, L. Zhang, L. Shi, P. Wang, *ACS Nano* **2017**, *11*, 3752.
[52] X. Fan, Y. Ding, Y. Liu, J. Liang, Y. Chen, *ACS Nano* **2019**, *13*, 8124.
[53] M. Naguib, M. W. Barsoum, Y. Gogotsi, *Adv. Mater.* **2021**, 2103393.
[54] C. J. Zhang, S. Pinilla, N. McEvoy, C. P. Cullen, B. Anasori, E. Long, S.-H. Park, A. Seral-Ascaso, A. Shmeliov, D. Krishnan, C. Morant, X. Liu, G. S. Duesberg, Y. Gogotsi, V. Nicolosi, *Chem. Mater.* **2017**, *29*, 4848.
[55] D. Boyer, P. Tamarat, A. Maali, B. Lounis, M. Orrit, *Science* **2002**, *297*, 1160.
[56] Y. Liu, S. Yu, R. Feng, A. Bernard, Y. Liu, Y. Zhang, H. Duan, W. Shang, P. Tao, C. Song, T. Deng, *Adv. Mater.* **2015**, *27*, 2768.
[57] X. Wu, G. Y. Chen, W. Zhang, X. Liu, H. Xu, *Adv. Sustainable Syst.* **2017**, *1*, 1700046.
[58] X. Wang, L. Yang, P. Yang, W. Guo, Q.-P. Zhang, X. Liu, Y. Li, *Sci. China: Chem.* **2020**, *63*, 1295.
[59] D. F. Cheng, C. Urata, M. Yagihashi, A. Hozumi, *Angew. Chem., Int. Ed.* **2012**, *51*, 2956.

© 2022 Wiley-VCH GmbH

[60] A. Tuteja, W. Choi, M. Ma, J. M. Mabry, S. A. Mazzella, G. C. Rutledge, G. H. McKinley, R. E. Cohen, *Science* **2007**, *318*, 1618.
[61] H. Wang, Y. Xue, J. Ding, L. Feng, X. Wang, T. Lin, *Angew. Chem., Int. Ed.* **2011**, *50*, 11433.
[62] J. Zhang, S. Seeger, *Angew. Chem., Int. Ed.* **2011**, *50*, 6652.
[63] X. Deng, L. Mammen, H. J. Butt, D. Vollmer, *Science* **2012**, *335*, 67.
[64] S. Pan, R. Guo, M. Bjornmalm, J. J. Richardson, L. Li, C. Peng, N. Bertleff-Zieschang, W. Xu, J. Jiang, F. Caruso, *Nat. Mater.* **2018**, *17*, 1040.
[65] H. Bellanger, T. Darmanin, E. Taffin de Givenchy, F. Guittard, *Chem. Rev.* **2014**, *114*, 2694.
[66] A. Takahara, N. Morotomi, S. Hiraoka, N. Higashi, T. Kunitake, T. Kajiyama, *Macromolecules* **1989**, *22*, 617.
[67] J. Wang, G. Mao, C. K. Ober, E. J. Kramer, *Macromolecules* **1997**, *30*, 1906.
[68] Y. Katano, H. Tomono, T. Nakajima, *Macromolecules* **1994**, *27*, 2342.
[69] A. Y. Fadeev, T. J. McCarthy, *Langmuir* **1999**, *15*, 3759.
[70] M. Rabnawaz, G. Liu, H. Hu, *Angew. Chem., Int. Ed.* **2015**, *54*, 12722.
[71] P. Liu, H. Zhang, W. He, H. Li, J. Jiang, M. Liu, H. Sun, M. He, J. Cui, L. Jiang, X. Yao, *ACS Nano* **2017**, *11*, 2248.
[72] M. Rabnawaz, G. Liu, *Angew. Chem., Int. Ed.* **2015**, *54*, 6516.
[73] C. Urata, B. Masheder, D. F. Cheng, A. Hozumi, *Langmuir* **2013**, *29*, 12472.
[74] L. Wang, T. J. McCarthy, *Angew. Chem., Int. Ed.* **2016**, *55*, 244.
[75] L. Jiang, Y. Zhao, J. Zhai, *Angew. Chem., Int. Ed.* **2004**, *116*, 4438.
[76] A. J. Meuler, G. H. McKinley, R. E. Cohen, *ACS Nano* **2010**, *4*, 7048.
[77] J. Chen, J. Liu, M. He, K. Li, D. Cui, Q. Zhang, X. Zeng, Y. Zhang, J. Wang, Y. Song, *Appl. Phys. Lett.* **2012**, *101*, 111603.
[78] Y. Liu, L. Moevius, X. Xu, T. Qian, J. M. Yeomans, Z. Wang, *Nat. Phys.* **2014**, *10*, 515.
[79] M. Liu, S. Wang, L. Jiang, *Nat. Rev. Mater.* **2017**, *2*, 17036.
[80] Z. Dong, M. F. Schumann, M. J. Hokkanen, B. Chang, A. Welle, Q. Zhou, R. H. A. Ras, Z. Xu, M. Wegener, P. A. Levkin, *Adv. Mater.* **2018**, *30*, 1803890.
[81] D. Wang, Q. Sun, M. J. Hokkanen, C. Zhang, F. Y. Lin, Q. Liu, S. P. Zhu, T. Zhou, Q. Chang, B. He, Q. Zhou, L. Chen, Z. Wang, R. H. A. Ras, X. Deng, *Nature* **2020**, *582*, 55.
[82] T.-S. Wong, S. H. Kang, S. K. Y. Tang, E. J. Smythe, B. D. Hatton, A. Grinthal, J. Aizenberg, *Nature* **2011**, *477*, 443.
[83] P. Kim, T.-S. Wong, J. Alvarenga, M. J. Kreder, W. E. Adorno-Martinez, J. Aizenberg, *ACS Nano* **2012**, *6*, 6569.
[84] P. W. Wilson, W. Lu, H. Xu, P. Kim, M. J. Kreder, J. Alvarenga, J. Aizenberg, *Phys. Chem. Chem. Phys.* **2013**, *15*, 581.
[85] S. Peppou-Chapman, J. K. Hong, A. Waterhouse, C. Neto, *Chem. Soc. Rev.* **2020**, *49*, 3688.

© 2022 Wiley-VCH GmbH